JOURNAL OF GEOPHYSICAL RESEARCH, VOL. 94, NO. B11, PAGES 15,521–15,539, NOVEMBER 10, 1989

Rupture Characteristics of the 1982 Tonga and 1986 Kermadec Earthquakes

PAUL R. LUNDGREN[1]

Istituto Nazionale di Geofisica, Roma, Italy

EMILE A. OKAL

Department of Geological Sciences, Northwestern University, Evanston, Illinois

DOUGLAS A. WIENS

Department of Earth and Planetary Sciences, Washington University, St. Louis, Missouri

Source time functions are obtained for the December 19, 1982, Tonga and October 20, 1986, Kermadec earthquakes from deconvolution of P waves, using a model including a significant dip of the ocean bottom. In such a geometry, the amplitudes of subsequent water multiples are large and irregular. As a result, we can model these two events as consisting of a single pulse of short duration (23 s in the case of the 1982 event, and 19 s for the 1986 one), despite complex teleseismic waveshapes. This is in contrast to inversions using flat-layered models, which required very complex source time functions, which were mutually inconsistent at different stations. The anomalously large tsunami generated by the 1982 event is modeled as the result of propagation of the rupture into the sedimentary wedge at the trench, rather than due to a long-lived complex source time function, the latter being also incompatible with the total lack of excitation of the Earth's normal modes in the low-frequency limit. For the 1986 event, we derive a source duration (19 s) very short in relation to its moment (8×10^{27} dyn-cm). This earthquake, a high stress drop rupture featuring a unique combination of strike-slip and thrust motion on a plane dipping oceanwards of the trench, is interpreted as expressing internal deformation of the subducting Pacific slab at a depth of 40 km, under the compressional stresses resulting from the collision.

1. INTRODUCTION

Much attention has recently been focused on understanding the rupture characteristics of large earthquakes. Body-wave deconvolution of the earthquake source time function has been the primary source of information on source duration and complexity, which in turn is interpreted in terms of stress heterogeneity along the fault plane, for example in the asperity [*Lay and Kanamori*, 1981] or barrier [*Aki*, 1979] formalisms. Such detailed studies, and the precise mapping of sub-events on the fault plane [*Houston*, 1987] are important for tectonic interpretation of large earthquakes [*Kikuchi and Kanamori*, 1982; *Ruff and Kanamori*, 1983; *Christensen and Lay*, 1988; *Lundgren and Okal*, 1988]. However, in recent studies, *Wiens* [1987] and *Lundgren et al.* [1988] have questioned the robustness of some solutions featuring very complex sources. In other words, some individual pulses in apparently very complex sources may be the spurious result of the use of inadequate models, most notably of an incorrect Green's function. Examples include modeling the event at the wrong depth, or ignoring changes in the focal geometry during rupture.

In the present study, we examine the effect of a dipping near-source structure on body-wave deconvolution in the case of two shallow subduction events. Specifically, following *Wiens* [1987, 1989], we show that very simple source functions can be derived for the earthquakes studied, by simply incorporating reflections at the dipping interfaces into the Green's function.

The two events selected for the analysis are the December 19, 1982 Tonga, and the October 20, 1986 Kermadec earthquakes. The former was chosen on the basis of the anomalously large tsunami generated and previous suggestions of possible rupture complexity. The 1986 Kermadec earthquake was selected on the basis of its unusual focal mechanism, featuring a significant amount of strike-slip motion which is not readily interpreted as expressing subduction of the Pacific plate under the Australian one. In addition, estimates of mantle magnitudes and seismic moments for this event have been significantly scattered [*Okal and Talandier*, 1987, 1989; *Romanowicz*, 1988; *Dziewonski et al.* 1987].

2. METHODS

We use the least-squares method developed by *Lundgren et al.* [1988] and incorporate the possible

[1]Now at Jet Propulsion Laboratory, Pasadena, California.

Paper number 89JB01221.
0148-0227/89/89JB-01221$05.00

effects of dipping near-source structure on the Green's function. Most previous deconvolution algorithms used a near-source structure modeled as horizontal layers of ocean, sediment, and oceanic crust, over a mantle half-space. This worked well for relatively deep events, such as as the the 1978 Kurile and 1977 Tonga earthquakes, which were located arc-wards from the oceanic trench, in an area where the ocean-crust interface is essentially flat [*Lundgren et al.*, 1988; *Christensen and Lay*, 1988; *Lundgren and Okal*, 1988]. However, Figure 1 shows that the 1982 and 1986 earthquakes are located directly under the steepest slopes from the island arc into the trench; thus the assumption of horizontal layering above the source may not be valid. For a shallow event on the flanks of the Cocos ridge, *Wiens* [1987] showed that an ocean floor slope of only 1.2° was sufficient to explain the observation of large and irregular water multiples. In turn, this allowed modeling the Cocos earthquake with a simple source time function whereas in the case of a flat-layered structure, the complex waveshapes might have been interpreted as the effect of source complexity. A later study proved that a dipping interface showed large observable effects for shallow subduction earthquakes in the Kurile trench [*Wiens*, 1989]. In the case of the inner slope of the Tonga-Kermadec oceanic trench, where the dip of the ocean bottom can approach 6° in some places, even greater effects can be expected.

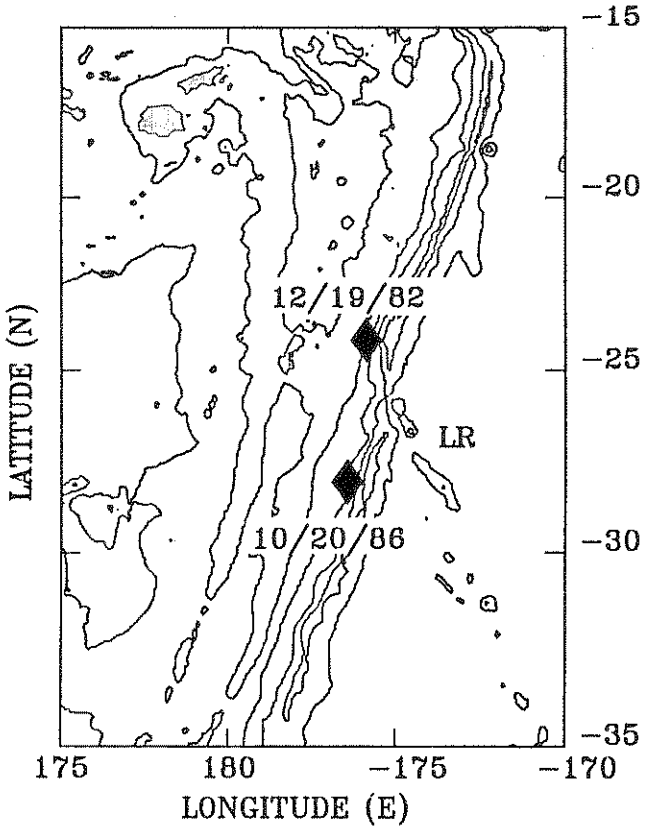

Fig. 1. Sketch of the Tonga-Kermadec Trench, showing the location of the two earthquakes studied (diamonds). Bathymetry is contoured at 2000 m intervals, with land areas shaded in gray. The Louisville Ridge is identified (LR).

In order to include such water multiples in the synthetic wavelets, we use geometric ray theory, following the method of *Wiens* [1987, 1989]. This algorithm computes teleseismic waveforms for a double-couple source in a structure consisting of any number of layers with arbitrarily dipping interfaces. For a given station, the *P* wave take-off angle at the source is calculated by following a ray with appropriate slowness in reverse direction from the receiver to the source along a specified ray path. Except in the case of stations located exactly updip or downdip, reflection off a dipping layer will result in a change of azimuth, and thus our procedure determines not only the take-off angle but also the azimuthal direction in which the ray leaves the source. The initial ray amplitude is computed from this orientation of the initial ray vector on the focal sphere. The ray is then traced forward through the predetermined number of water and crustal bounces. For each bounce the time delay, geometric spreading, and plane wave reflection and transmission coefficients are computed. When rays are incident past their critical angle, the transmission and reflection coefficients, and amplitudes, become complex. After all the reflections and transmissions from source to receiver are computed, the imaginary part of the amplitude is convolved with the Hilbert transform of a δ-function, and both the real and imaginary parts are convolved with attenuation and instrument operators [*Choy and Richards*, 1975; *Langston*, 1977].

Water multiples have a large effect on the waveform because of the large impedance contrast at the ocean bottom, so that significant energy is retained after several reverberations in the water column [*e.g., Ward*, 1979; *Stein and Wiens*, 1986]. Because of the dipping ocean floor, rays which would normally lie in the plane of the great circle from source to receiver independently of the number of reflections, can change azimuth with each reflection or transmission at a dipping interface. For stations which have nodal direct *P* waves, the water multiples, which take off in the upper focal hemisphere, can originate at a different azimuth, and possibly with much higher amplitudes. More generally, because of the variability of the take-off angles of the water multiples, a later reverberation may suddenly show a large amplitude. Thus, the water multiples may not show a monotonic decrease in amplitude with time, as for a flat-layered structure [*Wiens*, 1987].

Procedure

In general, single-station inversions are very successful at producing synthetics which fit the data almost exactly. However, a serious problem with single-station deconvolution of multiple-station datasets is that it can occasionally lead to substantially different source time functions at the various stations [*e.g., Christensen and Lay*, 1988]. Such discrepancies, for example in source complexity and duration, are powerful indicators of the use of an inadequate Green's function. On the other hand, multiple-station deconvolutions do not fit the individual seismograms as well as when they are inverted separately, a simple expression of the obvious fact that the dimension of the data space is increased considerably in a multiple-

station inversion, while the parameter space remains unchanged. In addition, multiple-station inversions do not perform well in the presence of significant source finiteness.

In the present study, we start off by carrying out single-station inversions of the dataset, and analyzing the coherence of the resulting various source time functions. We identify large azimuthal variations in their complexity, especially between stations located near the nodal planes, and in the center of the focal quadrants. These inconsistencies point out the necessity of using a different model. In accordance with the local bathymetry, we introduce dipping interfaces, and then proceed with a multiple-station inversion, using this more realistic model.

3. THE DECEMBER 19, 1982 TONGA EARTHQUAKE

Background

Epicentral parameters for this large shallow thrust earthquake are given by the International Seismological Centre (ISC) as 24.15°S, 175.97°W, and 17:43:57.5 UT. The depths reported for this event range from 29 km for the centroid moment tensor (CMT) solution [*Dziewonski et al.*, 1983] to 40 km (ISC). The magnitudes reported are $m_b = 5.9$; $M_s = 7.5$ by the ISC, and $m_b = 5.9$; $M_s = 7.7$ by the National Earthquake Information Service (NEIS). Estimates of the seismic moment of the earthquake are 0.9 to 2.0×10^{27} dyn-cm [*Dziewonski et al.*, 1983; *Christensen and Lay*, 1988]. Mantle magnitudes (theoretically equivalent to $\log_{10} M_0 - 20$) reported by *Okal and Talandier* [1989] usually agree with these figures: $M_m = 7.47$ (spectral domain) and 7.28 (time domain) at Papeete, Tahiti (PPT), 7.14 at Pasadena (PAS), and 7.36 at the GEOSCOPE station PCR on Réunion Island. A major problem with this event is that its tsunami (14 cm peak-to-peak at PPT) is 8 times larger than would be expected from published estimates of its seismic moment [*Okal*, 1988; *Talandier and Okal*, 1989]. Indeed, the tsunami is comparable in amplitude to that of the much larger June 22, 1977, Tonga event, which had a moment of at least 1.4×10^{28} dyn-cm [*Talandier and Okal*, 1979; *Lundgren and Okal*, 1988], the disparity in seismic amplitude between the two events being illustrated in Figure 2. As such, the 1982 event qualifies as a so-called "tsunami earthquake", as defined by *Kanamori* [1972] or *Fukao* [1979].

Rupture complexity for this event was suggested in initial PDE reports. More recently, *Christensen and Lay* [1988] carried out individual station body-wave deconvolutions, which yielded complex time functions featuring many distinct source pulses, but with a general loss of coherence beyond 30 s into the signal. Thus, they suggest a total duration of 28 s, and an average moment of 0.9×10^{27} dyn-cm.

Since the amplitude of the tsunami is controlled primarily by the low-frequency value of the seismic moment [*Abe*, 1973; *Okal*, 1988], we further explored the possibility that this earthquake may have an extremely slow, very large component to its source, which would have been missed by studies based exclusively on body waves. In Figure 3, we compare the complex spectra of IDA records, at the same station NNA, of the June 22, 1977 and December 19, 1982 Tonga events. Both time windows start approximately 6 hours after the event and last 655,360 s. It is clear that the 1982 event failed to excite the Earth's normal modes above noise level in the precise frequency range (1–2 mHz) corresponding to the excitation of the reported tsunami. Given the higher noise level on the amplitude spectrum in 1982, the phase spectrum evidence is particularly compelling. The lack of energy release in the source spectrum at these frequencies means that the large tsunami amplitude of the 1982 earthquake

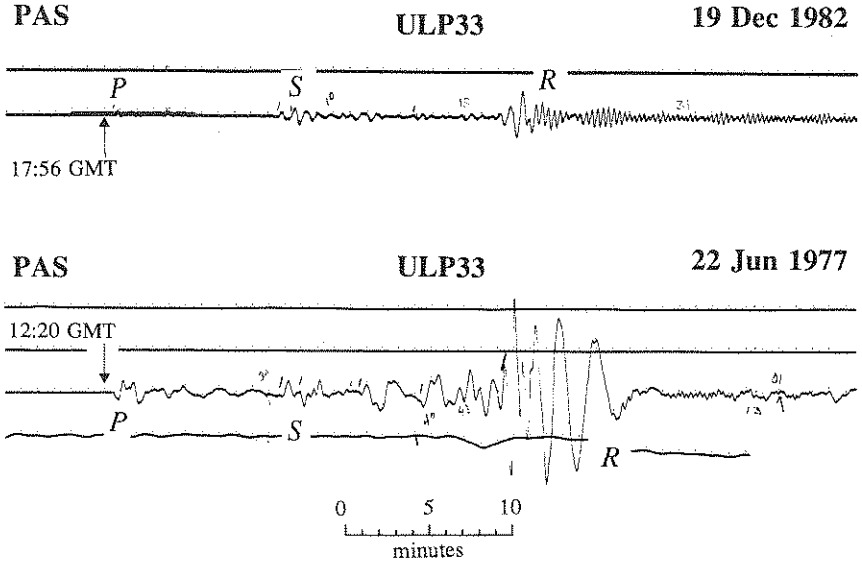

Fig. 2. Comparison of the Pasadena ultra-long period records of the 1977 and 1982 Tonga earthquakes. The disparity in seismic moment is obvious from these records.

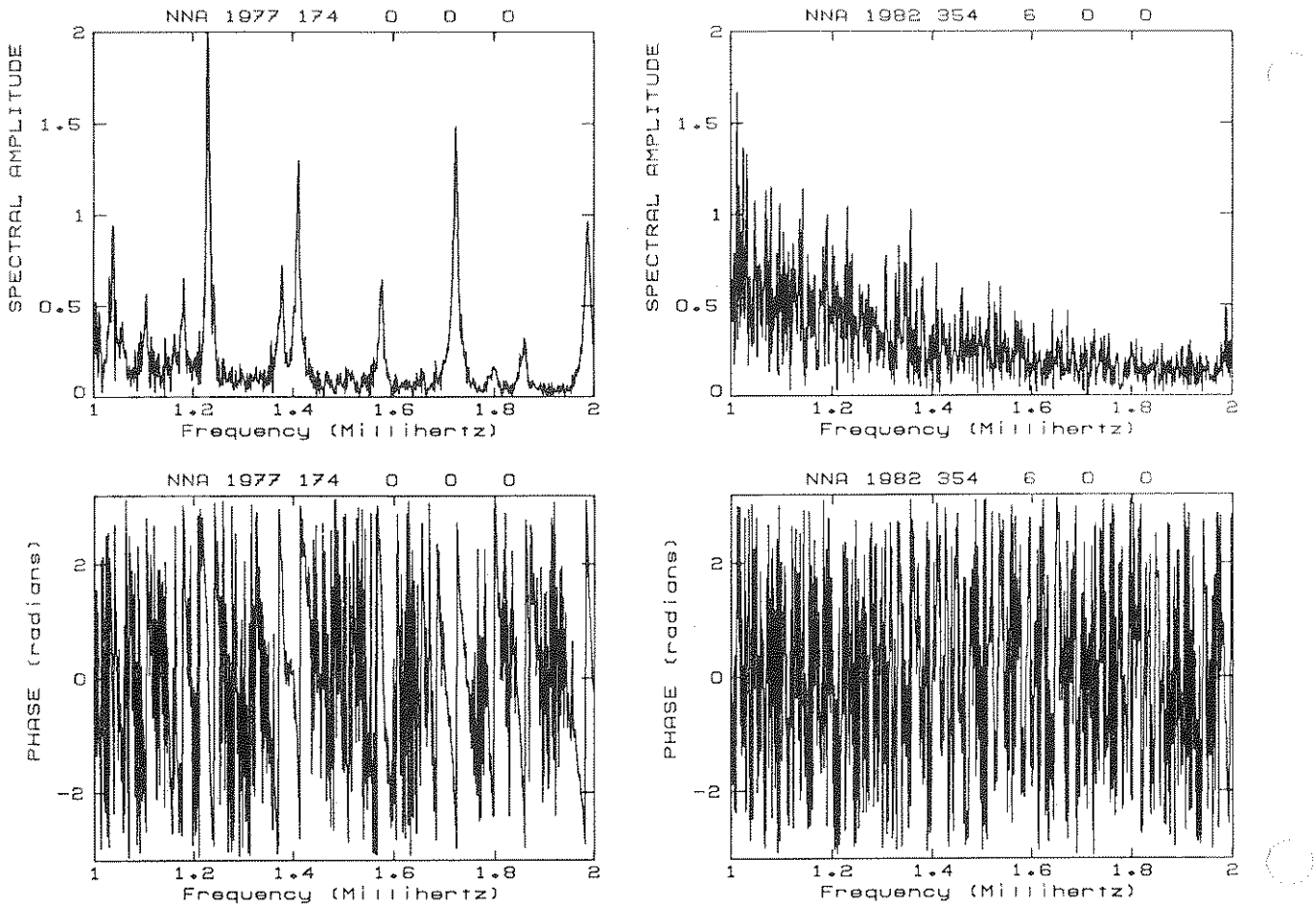

Fig. 3. Comparison of Fourier spectra at the Ñaña IDA station for the 1977 (left) and 1982 (right) Tonga earthquakes. (Top): Amplitude spectra. (Bottom) Phase spectra. For the 1982 spectra, note the absence of detection of any normal mode above noise level in the frequency range characteristic of tsunami excitation. The windows and scales are the same for both events; see details in text.

is not due to an extra-slow component of its source, but rather to an anomalously high ratio of tsunami versus seismic excitation.

Figure 4 shows the focal mechanism obtained from the CMT solution [*Dziewonski et al.*, 1983]. It consists of a shallow-dipping thrust fault, interpreted as expressing the under-thrusting of the Pacific plate under the Australian plate. This mechanism was also used by *Christensen and Lay* [1988].

Body Wave Modeling

We used *P* wave seismograms from eight stations: NWAO, CTAO, TATO, GUMO, COL, LON, JAS, ANMO, well distributed in azimuth. Table 1 lists all pertinent parameters of the source receiver geometry. Figure 5 shows the *P* waves used for each of the stations.

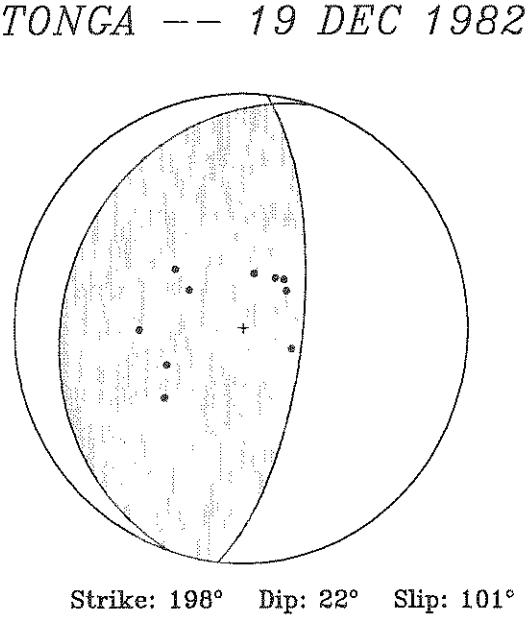

Fig. 4. Focal mechanism of the December 19, 1982, Tonga earthquake. First motion picks (all compressional) are from this study; focal planes as given by the Harvard CMT solution [*Dziewonski et al.*, 1983].

TABLE 1. Geometry of Stations Used in the Present Study

Code	Station	Network or Instrument	Distance (deg)	Azimuth From Source (deg)
	Tonga, December 19, 1982			
	Body-Wave Modeling			
CTAO	Charter Towers, Queensland, Australia	GDSN	35.15	268.99
GUMO	Agana, Guam	GDSN	53.59	310.20
NWAO	Narrogin, Western Australia	GDSN	58.43	244.99
TATO	Taipei, Taiwan	GDSN	77.87	304.42
JAS	Jamestown, California	GDSN	80.93	41.40
LON	Longmire, Washington	GDSN	85.97	34.05
ANMO	Albuquerque, New Mexico	GDSN	88.33	50.46
COL	College, Alaska	GDSN	91.54	11.65
	Kermadec, October 20, 1986			
	Body-Wave Modeling			
MAJO	Matsushiro, Japan	GDSN	77.35	323.89
JAS	Jamestown, California	GDSN	84.15	41.28
ANMO	Albuquerque, New Mexico	GDSN	91.14	50.63
CHTO	Chiengmai, Thailand	GDSN	94.19	288.81
COL	College, Alaska	GDSN	95.49	11.46
ZOBO	Zongo, Bolivia	GDSN	97.71	113.15
BOCO	Bogota, Colombia	GDSN	103.01	91.90
	Kermadec, October 20, 1986			
	Mantle Rayleigh Waves			
NOC	Nouméa, New Caledonia	GEOSCOPE	16.80	286.75
PPT	Papeete, Tahiti, French Polynesia	GEOSCOPE	26.77	72.70
PAF	Port-aux-Français, Kerguelen Is.	GEOSCOPE	82.69	217.13
PAS	Pasadena, California	ULP33	82.99	45.36
WFM	Westford, Massachusetts	GEOSCOPE	116.85	54.23
SSB	Saint-Sauveur de Badole, France	GEOSCOPE	162.84	357.83

A significant difference of waveshape is immediately apparent between stations located west and east of the meridian of the epicenter. Stations to the west have *P* waves which are simpler in shape and have much less "ringing" (presumably water multiples) than those to the east, which also are somewhat shorter in period.

As a first step, single-station deconvolutions were performed with a near-source structure consisting of a 4 km water layer, 1 km of sediment, and 6 km of oceanic crust over a half-space. At the western stations (NWAO, CTAO, TATO, and GUMO), this yielded a simple source time function consisting of a single pulse, but at the North American stations, the source time functions were of overall longer duration, and composed of several pulses of shorter duration with substantial amounts of negative moment release.

When trying to invert simultaneously the whole dataset, we found that stations in each of these two groups could be successfully inverted together to find a common source time function (Figure 6). But if stations from both groups were inverted together (Figure 7), the western stations would dominate the inversion, producing synthetics which matched its dataset but gave a very poor fit for the eastern stations. Thus, while each group is internally consistent, the two groups are not compatible with each other.

The solution to the problem was the introduction of dipping layers in the near-source structure of the eastern stations. In practice this involved inverting the complete dataset over a range of layer dip angles, strikes of the dipping layers, and water layer thicknesses. The structure which we found worked best was a water depth of 4 km, with an ocean bottom dipping 3° at a strike of N20°E. Table 2 gives all relevant structural parameters. The dataset was then inverted over a range of depths to find the depth and source time function with the least error.

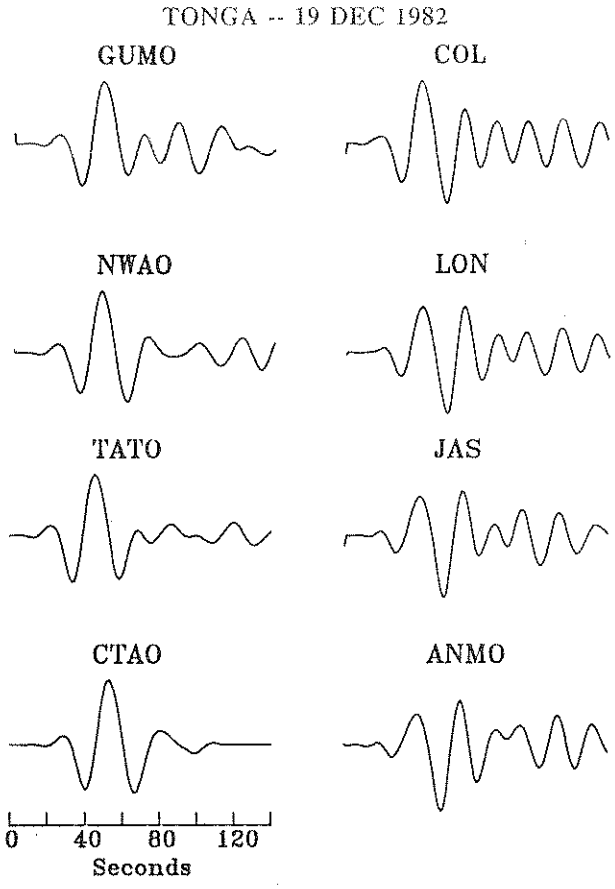

Figure 8*a* shows the comparison of the synthetics to the data. We find an excellent fit to all eight seismograms, especially at the North American stations. The resulting moment, 1.4×10^{27} dyn-cm, is in general agreement with the figures quoted above. However, the source time function computed from the complete dataset is a single pulse 23 s in duration (Figure 8*b*). This source time function is also remarkably free of negative values of the seismic moment release rate.

Discussion

The value of the seismic moment obtained in the present investigation is not significantly different from those published in previous studies. Our depth (20 km) is somewhat less than the 25 km obtained by *Christensen and Lay* [1988], or the 29 km of the Harvard CMT solution [*Dziewonski et al.*, 1987], and lower than the 40 km reported by the ISC. The fundamental result from our study is that, once an adequate structural model is used in the source region, the seismic source time function turns out to be a simple pulse.

Fig. 5. GDSN seismograms used for the 1982 Tonga earthquake. Stations in the left column (located westwards of the epicenter) have simpler waveforms than those in the right column (located eastwards of the source).

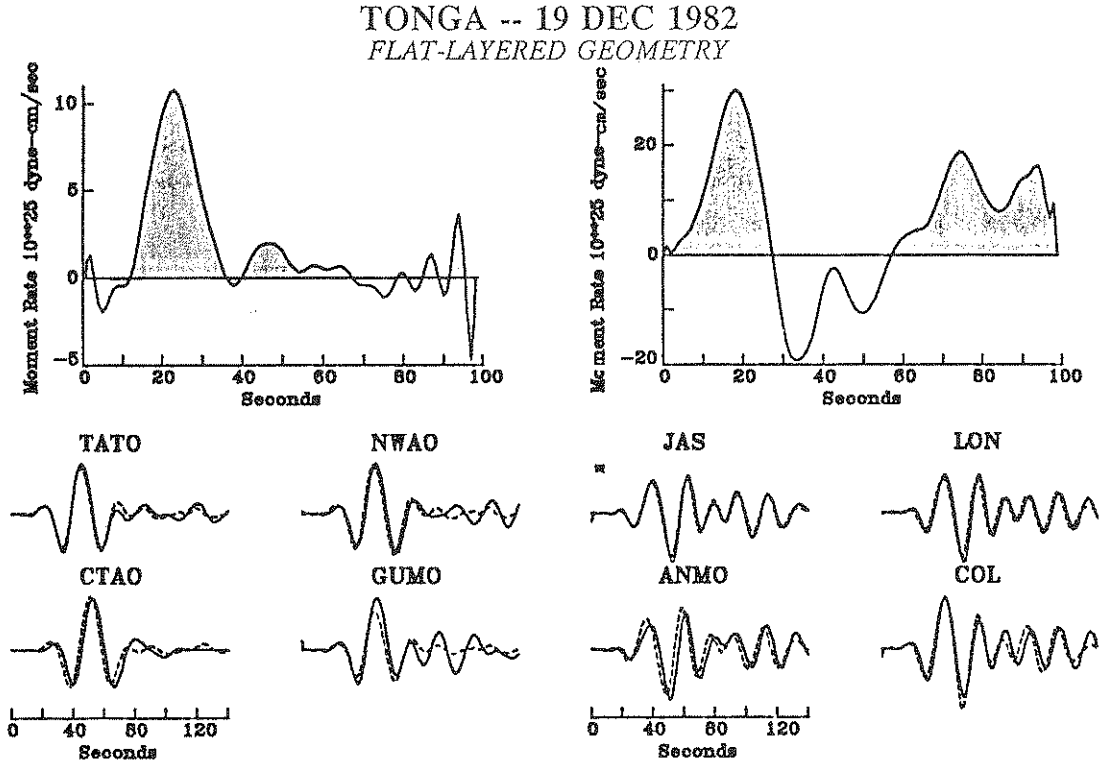

Fig. 6. Comparison of the source time functions and fits of synthetics to data for the western (left) and eastern (right) groups of stations for the 1982 Tonga earthquake. A flat-layered geometry is used, and a four-station sub-dataset is inverted simultaneously for both cases. The resulting moment rate time functions for both experiments are shown at the top. Note that a good fit is obtained for either group, but that the two solutions become mutually inconsistent 30 s into the source time function.

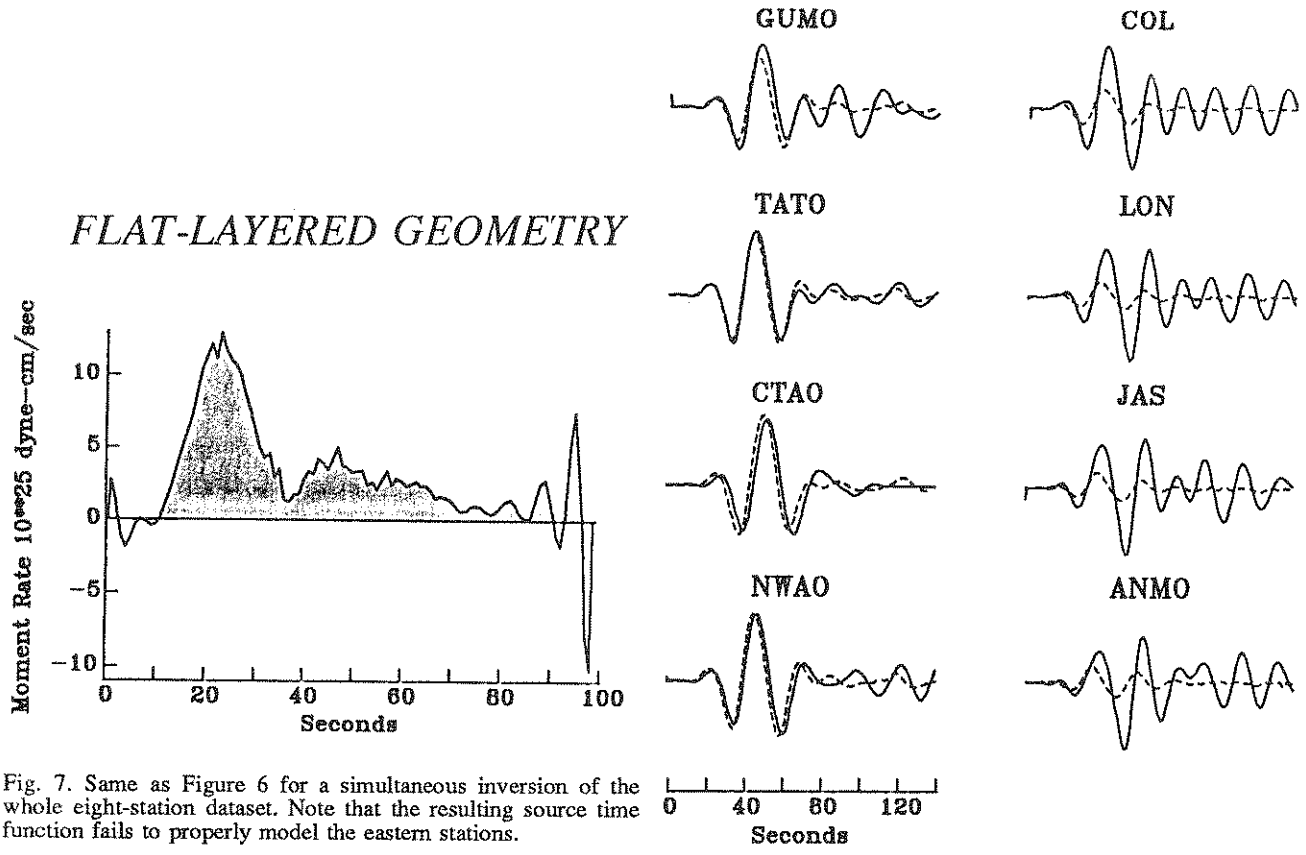

Fig. 7. Same as Figure 6 for a simultaneous inversion of the whole eight-station dataset. Note that the resulting source time function fails to properly model the eastern stations.

Geller [1976] and later *Kanamori and Given* [1981] have given models of the variation of the duration τ_s of the seismic source in relation to the seismic moment M_0. Geller assumes that subduction earthquakes scale at a constant stress drop $\Delta\sigma$, and obtains the relation $\tau_s = 18\, M_0^{1/3}$, where τ_s is in seconds and M_0 in units of 10^{27} dyn-cm. Kanamori and Given list an empirical model corresponding to a slightly slower release of seismic energy. Both of these models are shown on Figure 9. It is apparent that the 1982 Tonga earthquake,

TABLE 2. Structural Parameters of Dipping Models Used in Present Study

Layer	Nature	Thickness (km)	α (km/s)	β (km/s)	ρ (g/cm^3)	Top of Layer's Dip	
						Plunge (deg)	Azimuth
			Tonga, December 19, 1982				
1	Ocean	4.0	1.5	0.0	1.03	0.0	
2	Sediments	1.0	2.0	1.0	1.5	3.0	N110°E
3	Crust	∞	6.5	3.8	2.85	3.0	N110°E
			Kermadec, October 20, 1986				
1	Ocean	6.0	1.5	0.0	1.03	0.0	
2	Sediments	1.0	2.0	1.0	1.5	3.0	N110°E
3	Crust	∞	6.5	3.8	2.85	3.0	N110°E

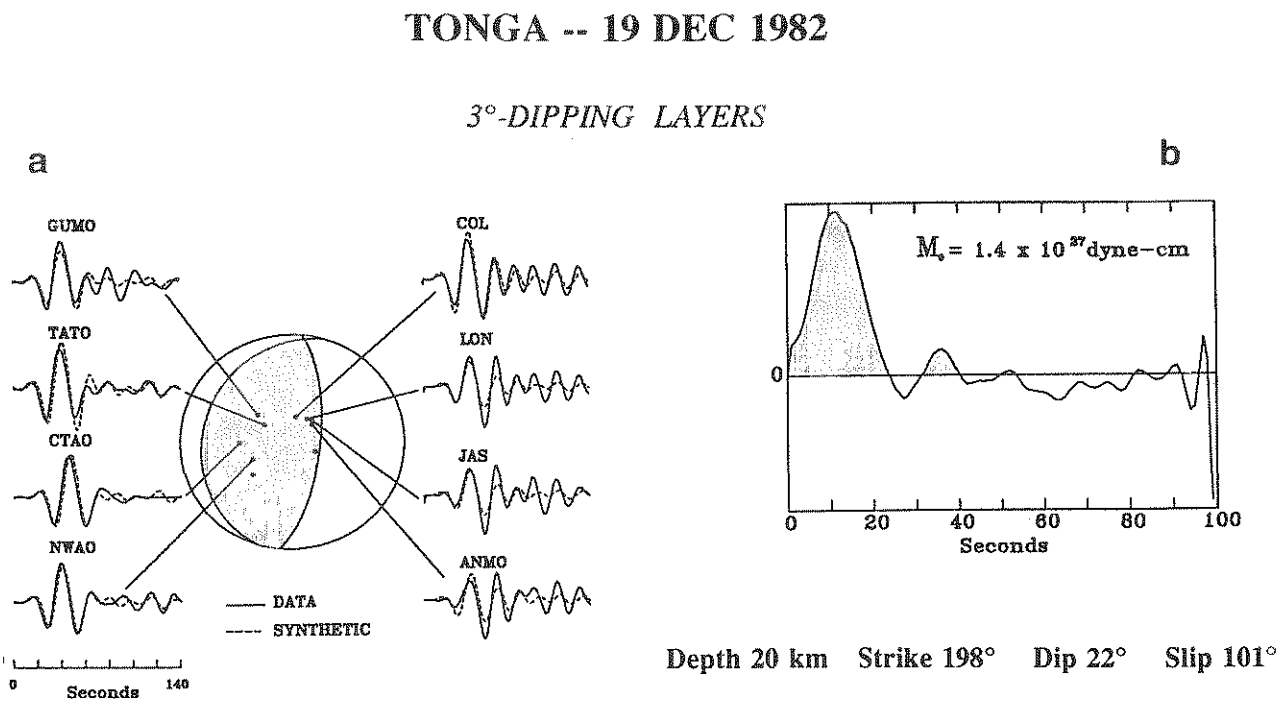

Fig. 8. *(a)* Comparison of data (solid) and synthetics (dashed) for a simultaneous inversion of the eight-station dataset, using a model 3°-dipping seafloor. *(b)* Resulting final source time function for the 1982 Tonga earthquake.

falling between the two curves, is in this respect in no way anomalous. Certainly, its very large tsunami cannot be explained by an unusually slow seismic source, a conclusion already reached from our normal mode study (Figure 3).

On the other hand, the 23 s duration of this event suggests that the characteristic dimension of its fault zone is about 70 km. The depth extent of the rupture can then be anywhere from 20 to 70 km, depending on the particular shape and orientation of the fault. Since our inversion yields a best depth of 20 km below sea level, actually only 10 km below the bottom of the trench, this strongly suggests that the 1982 Tonga event may have ruptured to the ocean floor. This would be in keeping with *Wiens'* [1989] recent observations, that two other tsunami earthquakes (the October 20, 1963 and June 10, 1975 events in the Kurile Islands) actually occurred at very shallow depths. In both the latter study and the present case of the 1982 Tonga event, this would necessarily involve a propagation of the rupture through the substantial accretionary prisms of sediments, documented to be overlying the trench in the focal areas.

In a recent review paper, *Okal* [1988] showed on theoretical grounds that the tsunamigenic excitation of a point source double-couple involving a dip-slip on a dipping fault plane (the so-called K_0 term in *Kanamori and Cipar*'s [1974] formalism) can be enhanced by as much as 2 orders of magnitude by placing the source in mechanically deficient material, such as sediments. As a consequence, the release of as little as a few percent of the total seismic moment inside a sedimentary prism is

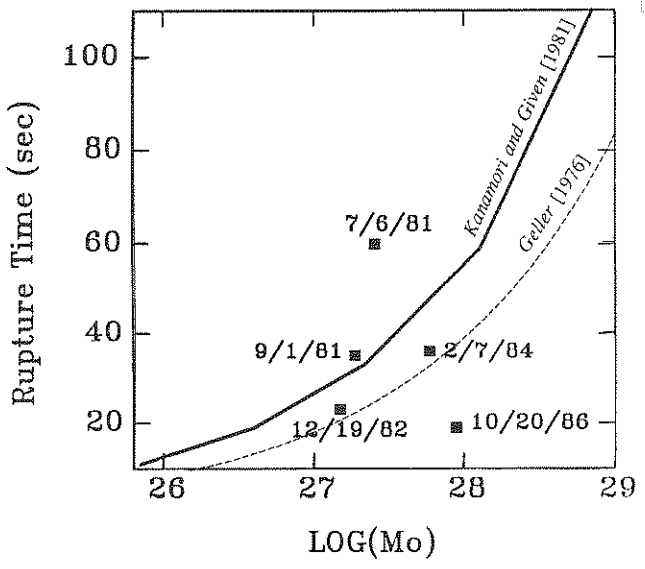

Fig. 9. Rupture duration plotted against moment for a number of large Southwest Pacific earthquakes [after *Lundgren*, 1988]. The solid curve is derived from *Kanamori and Given* [1981], and the dashed one from *Geller* [1976].

sufficient to boost the amplitude of the resulting tsunami by an order of magnitude. We believe that such a geometry can actually explain the anomalous tsunami of the 1982 Tonga earthquake. In Figure 10*a*, we compare synthetic marigrams computed at PPT for the 1977 and

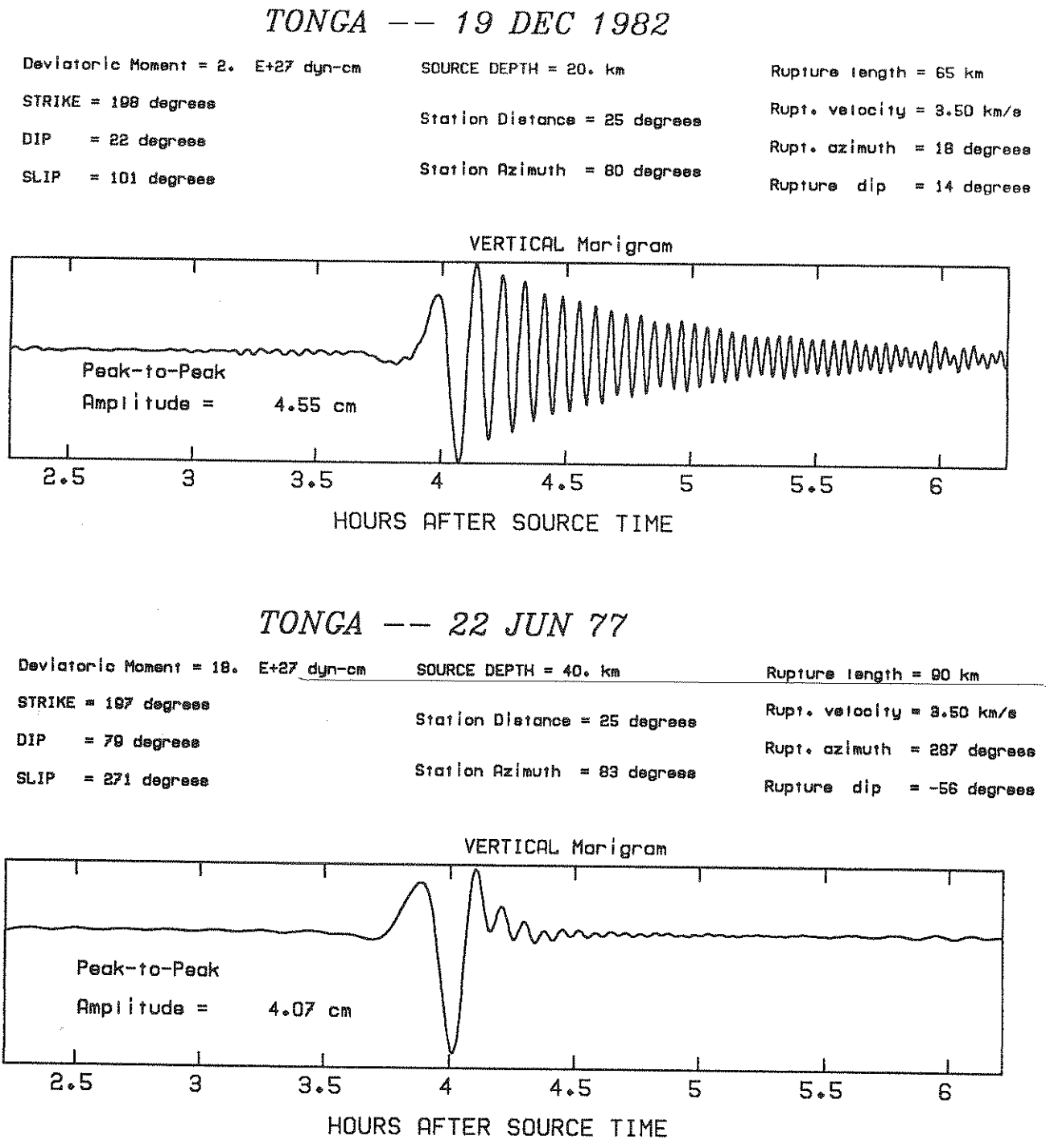

Fig. 10*a*. Synthetic marigrams for PPT, generated in the focal and rupture geometries of the 1982 (top) and 1977 (bottom) Tonga earthquakes. Note that despite strongly different moments, the resulting amplitudes are comparable.

1982 Tonga events, using the model of rupture of *Lundgren and Okal* [1988] for the 1977 event and, in the case of the 1982 earthquake, a rupture terminating 100 m below the water-sediment interface. Since our marigrams are computed on the high seas, and do not take into account the interaction of the tsunami with the receiving shore (the so-called "run-up" and resonance effects), it is not possible to compare directly the absolute amplitudes of the synthetics with those observed on the PPT harbor maregraph. However, their observed ratio (14:12 in favor of the 1982 event) is correctly predicted by our model, despite a ratio of seismic moments of between 7

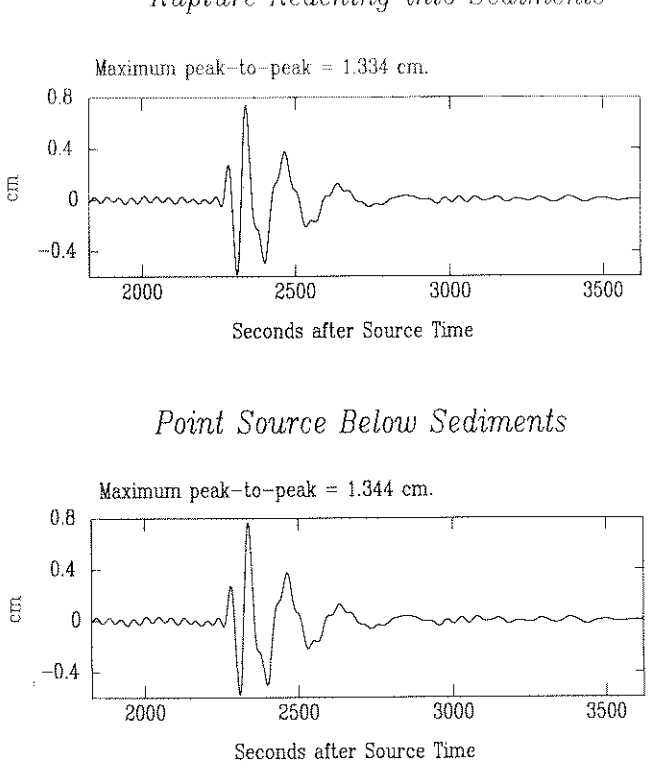

Fig. 10*b*. Synthetic seismograms of Rayleigh waves in the period range 40–300 s, generated for the 1982 event in the geometry of the Pasadena station. (Top) Rupture propagating from an initial depth of 20 km, upwards and into the sedimentary layer; this source is the same one used in the top frame of Figure 10*a*. (Bottom) Point source located at the centroid of the rupture (11.5 km). Note the similarity of waveshapes and amplitudes. The ULP-33 instrument response is included, and the moment is $M_0 = 2 \times 10^{27}$ dyn-cm in both cases.

and 14 in favor of the 1977 event (we use a ratio of 9 in our modeling). In addition, these synthetics correctly predict a higher frequency for the tsunami wave of the 1982 event. On the other hand, Figure 10*b* compares synthetic Rayleigh wave seismograms generated in the geometry of Pasadena for the same 1982 rupture as used in the marigram analysis (top), with those for a spatial and temporal δ-function (bottom), located at the centroid of the rupture (11.5 km depth). It is clear that neither the waveform, nor the amplitude of the resulting Rayleigh wave is affected substantially by the release of a minor fraction of the seismic moment inside the sedimentary layer.

4. THE OCTOBER 20, 1986 KERMADEC EARTHQUAKE

Background

This earthquake in the northern Kermadec arc is obviously much larger than the 1982 event. The PDE epicentral parameters are given as 28.12°S, 176.37°W and 06:46:09.9 UT. The NEIS depth for this event is 29 km from broadband displacement seismograms, and the CMT depth is reported as 50 km [*Dziewonski et al.*, 1987]. NEIS magnitudes for this earthquake are $m_b = 6.6$ and $M_s = 8.1$; Berkeley gives $M_s = 8.3$. The moment of this event is the subject of some controversy. The CMT solution is $M_0 = 4.5 \times 10^{27}$ dyn-cm, comparable to the moment, $M_0 = 5.1 \times 10^{27}$ dyn-cm, obtained by *Romanowicz* [1988]. However, mantle magnitudes for this earthquake are unusually high [*Talandier et al.*, 1987; *Okal and Talandier*, 1989]. The M_m value at PPT (7.98, much larger than the CMT value) is computed at an anomalously short period of 51 s. The PAS M_m value (7.94) is also high, but was computed at longer periods (227 s).

The event occurred towards the northern limit of the Kermadec seismic arc. The latter is separated from the Tonga arc by a region of reduced seismicity, apparent in Figure 11*a*. In this figure, we plot all earthquakes with depths shallower than 100 km, starting in 1963, and ending with the October 20, 1986 mainshock. The seismic deficiency observed between 25°S and 27°S has been attributed to the interaction of the Louisville Ridge with the subduction zone [*Kelleher et al.*, 1974]. Immediately to the North of the 1986 event, a gap exists in the seismicity, which is filled by the two-month aftershock distribution (Figures 11*b* and 11*c*). Note that the gap extends approximately 160 km in a NNE direction along the trench, but does not reach the zone of reduced seismicity corresponding to the Louisville ridge intersection.

Published focal mechanisms for the 1986 earthquake are the NEIS moment tensor solution ($\phi_f = 16°$; $\delta = 77°$; $\lambda = 66°$) and the Harvard CMT solution [*Dziewonski et al.*, 1987] ($\phi_f = 13°$; $\delta = 71°$; $\lambda = 36°$). First motion picks from GDSN *P*-wave data gathered in the present study fail to constrain the mechanism properly. On the basis of our body-wave deconvolutions, we favor the mechanism shown on Figure 12*c* ($\phi_f = 13°$; $\delta = 74°$; $\lambda = 45°$), which is basically intermediate between the two published solutions. The variation in slip angle between our preferred solution and the CMT one remains small, and does not suggest *a priori* a complex rupture involving a change in mechanism, for example due to reactivation of a decoupled fault zone, as suggested by *Tajima and Célérier* [1989]. As discussed later, this reactivation process may have been involved during the aftershock sequence, but our ability to model the mainshock with an extremely simple source time function makes it unlikely that reactivation took place during the main shock.

The mechanism of the October 20, 1986 event is anomalous in its large component of strike-slip. Figure 13 is a diagram of slip angles for all centroid moment tensor solutions published by the Harvard group [*Dziewonski et al.*, 1983] for shallow events having occurred between 1977 and 1986 in the area mapped in Figure 11*a*, and with a moment of at least 10^{25} dyn-cm. As expected, most slip angles are close to 90° on both fault planes, expressing reverse faulting at the subduction zone. A few events have slip vectors approaching 270° (notably the large June 22, 1977 Tonga earthquake), and correspond either to decoupling of the slab, or to outer rise buckling. Finally, three small earthquakes feature

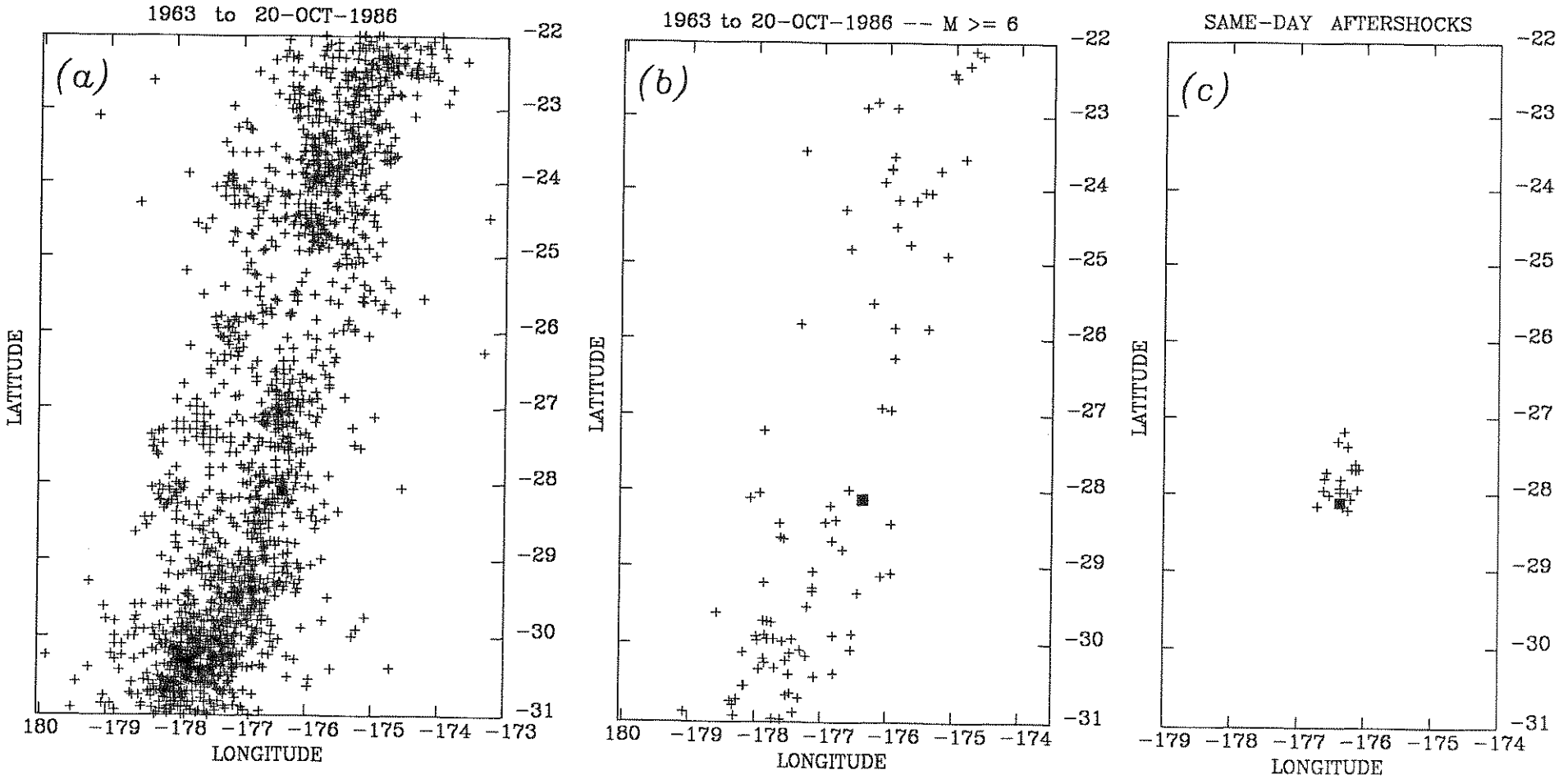

Fig. 11. Shallow seismicity of the Kermadec trench in the vicinity of the 1986 epicenter. *(a)* Earthquakes prior to the Kermadec main shock, with depths less than 100 km; note seismic deficiency at location of Louisville Ridge subduction. *(b)* Same as (a), but with magnitude threshold $M \geq 6$. Note seismic gap immediately to the North of the 1986 event. *(c)* Same-day, well-constrained aftershocks of the 1986 event (see text for details). In all frames, the 1986 main shock is shown as a solid square.

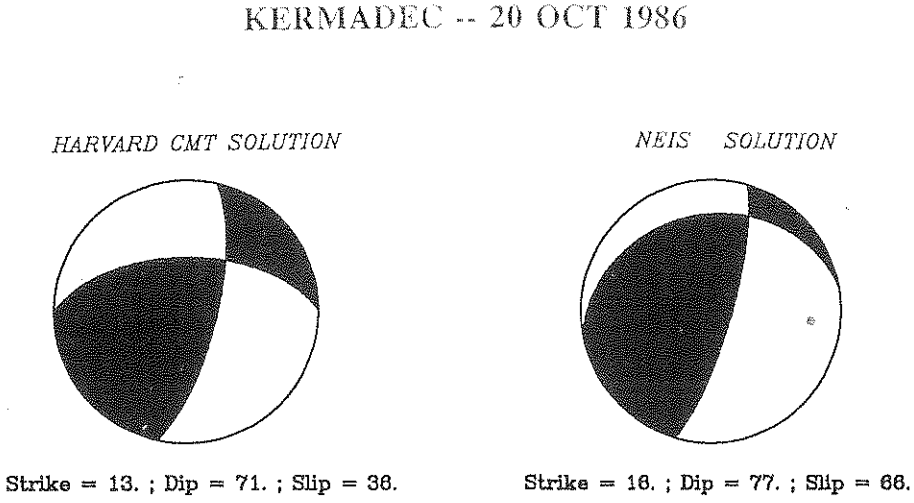

Fig. 12. Focal mechanism solutions for the 1986 Kermadec earthquake. (Top) CMT Solutions proposed by Harvard (left) and the NEIS (right). (Bottom) Preferred solution obtained in this study. Individual dots are compressional (solid) and dilatational (open) first motions read by the authors; the final focal planes are obtained by optimization of body-wave modeling.

nearly pure strike-slip; these events are located along the volcanic arc, i.e., significantly behind the subduction boundary. Strike-slip earthquakes in similar geometries have long been known in areas involving substantial obliquity of subduction [*Fitch*, 1972]. The only event in Figure 13 not falling in one the above categories is the 1986 Kermadec earthquake. Its large moment makes it all the more remarkable.

We further investigated the exceptional character of the mechanism of the 1986 Kermadec earthquake through a worldwide computer search of the Harvard CMT solutions for large shallow events (defined as $h \leq 100$ km; $M_0 \geq 10^{27}$ dyn-cm) with both slip angles in the 30–60° range ($\pm n$ 90°). This systematic effort turned out only five earthquakes in the period 1977-1987. Three of them (Samoa, 1977; Solomon, 1984; and New Ireland, 1983) correspond to oblique slip on a focal plane compatible with local subduction geometry; the fourth, an aftershock of the Chilean earthquake of 1985, should not be interpreted on a global scale. The fifth and last event is the 1986 Kermadec earthquake, the only one featuring a focal plane dipping oceanwards of the trench.

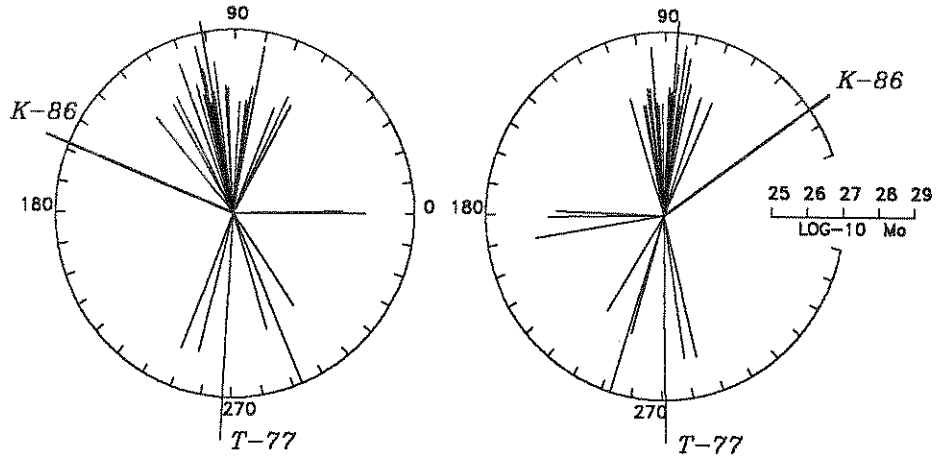

Fig. 13. Slip vector orientations from Harvard CMT focal solutions for Tonga-Kermadec events. Included are all events shallower than 90 km, with epicenters falling inside the map of Figure 11*a*, and with a moment of at least 10^{25} dyn-cm. Each event is plotted as a vector parallel to the orientation of the slip vector on the fault plane, and whose length is related to the seismic moment (see scale at right). The two diagrams correspond to the two possible fault solutions, the distinction being arbitrary, and each event being plotted twice. The 1977 Tonga and 1986 Kermadec earthquakes are identified; note that the latter is unique in that both slip angles are intermediate between dip- and strike-slip.

Body Wave Deconvolution

We were able to get good *P* wave records from seven stations, with an azimuthal distribution which includes only two stations to the west of the epicenter, but with two South American stations enhancing the distribution of stations to the east. As in the case of the 1982 Tonga earthquake, the *P* waves for this event show a distinct difference in waveform between western stations (CHTO and MAJO) and eastern ones (COL, JAS, ANMO, BOCO, and ZOBO). The North and South American stations do not show the simple waveforms of CHTO and MAJO, but rather have greater complexity, and are clearly higher in frequency. Again, this suggests that this earthquake's location directly under the inner slope of the trench may cause greater water reverberations later in the waveform at stations with azimuths in the direction of the trench.

Single-station deconvolutions resulted in a pattern similar to that of the 1982 event: at stations CHTO and MAJO, the use of a flat layered structure produced source time functions with a very simple, single pulse, similar to that for the December 19, 1982 event, though shorter in duration. The stations in the Americas gave source time functions with much greater complexity, significant portions of the source time function negative, and with significant moment release for the full duration of the deconvolved record (100 s). Stations CHTO and MAJO could be inverted together with very good agreement, but if other stations such as COL were added, the inversion was dominated by CHTO and MAJO, fitting synthetics to their *P* waveforms well and providing a very poor fit to COL. When inverted with the western stations, the eastern stations were never fit well, and their *P* wave seismograms were always much higher in frequency than the synthetics.

We resolved this inconsistency with a near-source structure composed of a shallow (3°) dipping ocean bottom, with dipping sediment and oceanic crust layers as well. As listed in Table 2, this near-source structure is the same as that for the 1982 event but with a slightly thicker water layer, 6 km deep. Figure 14*a* shows the error curve for a range of deconvolved source depths. The best fitting depth is 40 km. The dataset was then inverted at a range of slip values shown in Figure 14*b*. The preferred slip angle is 45°. Figure 15*a* shows the comparison of data and synthetics for the preferred solution. The source time function is shown in Figure 15*b* with a total duration of 19 s.

We derive a moment of (8.5 to 10) $\times 10^{27}$ dyn-cm. The lower value represents the single station inversion result for MAJO and the larger value is for both CHTO and MAJO inverted simultaneously. These stations were used to calculate the moment since they lie in a direction away from the trench and are adequately modeled with a flat-lying structure.

Discussion

The moment values obtained for the 1986 Kermadec earthquake are significantly larger than those published in the Harvard CMT solutions [*Dziewonski et al.*, 1987], but in general agreement with the large mantle magnitudes M_m obtained by *Okal and Talandier* [1989] both at PPT and PAS. Our second result is the short duration (τ_s = 19 s) of the source for an earthquake of this size. As shown in Figure 9, the combination of these two parameters suggests a very fast, "clean", stress release. Other estimates of the source duration vary from 30 s [*Dziewonski et al.*, 1987] to 50 s [*Romanowicz*, 1988].

In order to investigate further the combined values of the static moment of the earthquake and of its source duration, we studied systematically the spectral characteristics of first-passage Rayleigh wave trains at a number

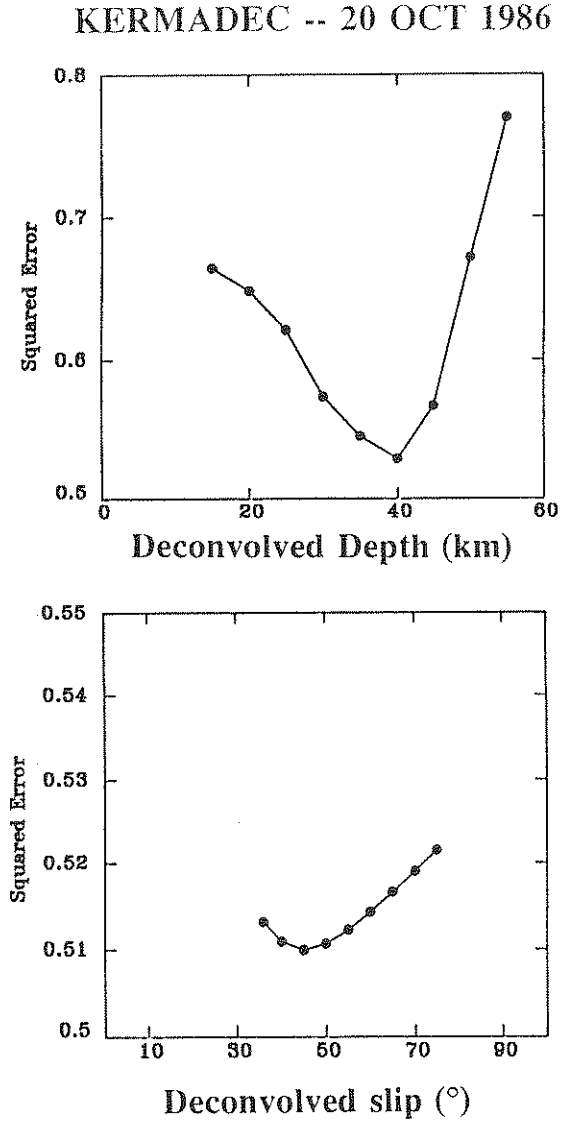

Fig. 14. Residual errors for simultaneous inversion of a seven-station dataset for the 1986 Kermadec event, using a model with dipping seafloor. (Top) The dataset is inverted at variable depths for the Harvard mechanism ($\phi = 13°$, $\delta = 74°$, $\lambda = 36°$). (Bottom) The depth is fixed at 40 km, and the dataset inverted at variable slip angles, yielding the best-fitting mechanism ($\lambda = 45°$).

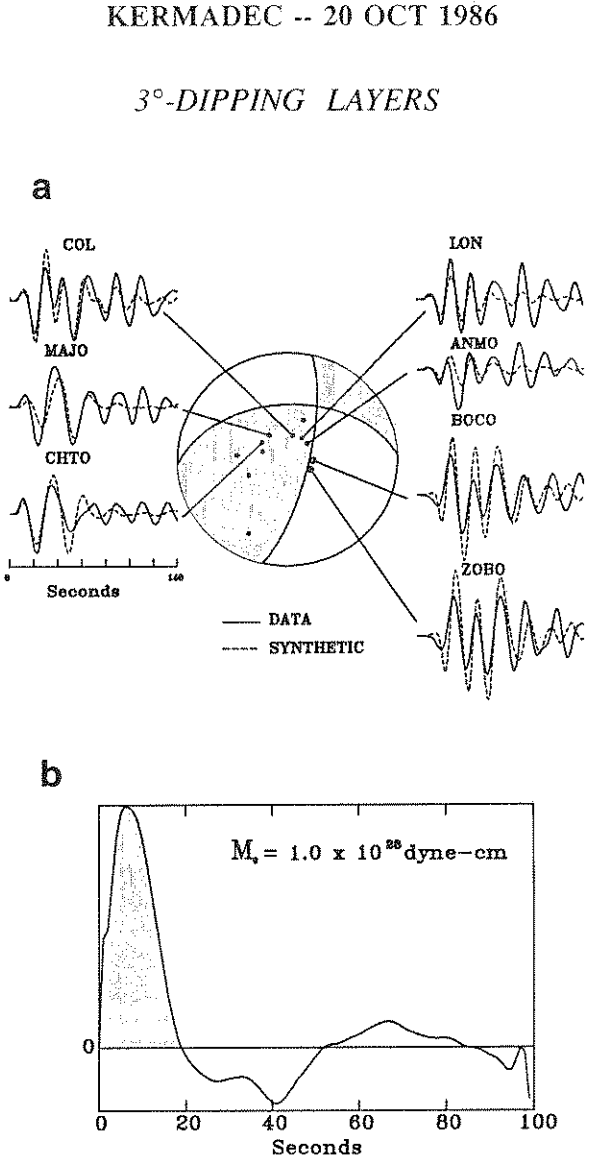

Fig. 15. Same as Figure 8 for the 1986 Kermadec event.

of GEOSCOPE stations, complemented by a record of the ultra-long period seismograph ("ULP 33") at Pasadena. We eliminated the antipodal station TAM and stations lying in a node of the radiation pattern (KIP, DRV, CRZ). We follow the general framework of *Okal and Talandier*'s [1989] mantle magnitude; at each station and for each frequency, we plot M_c, an expression of the mantle magnitude corrected for the exact geometry (depth; focal mechanism) of the source. This amounts to effecting all necessary corrections (source geometry, source excitation, propagation, and instrument response), and M_c should be expected to behave as

$$M_c = \log_{10} [\, M_0 \cdot \mathrm{sinc}\, \frac{\omega \tau_s}{2} \,] - 20 \qquad (1)$$

where M_0 is in units of 10^{27} dyn-cm. Results are presented in Figure 16. In each diagram, the solid line is the source spectral amplitude predicted by our model ($M_0 = 8.5 \times 10^{27}$ dyn-cm; $\tau_s = 19$ s), the dotted line is that predicted by the Harvard CMT solution ($M_0 = 4.6 \times 10^{27}$ dyn-cm; $\tau_s = 30$ s), and the long-dash line is that predicted by *Romanowicz*'s [1988] solution ($M_0 = 5.1 \times 10^{27}$ dyn-cm; $\tau_s = 50$ s). GEOSCOPE data, sampled at 10 s intervals, cannot be used beyond 0.016 Hz; the PAS data was digitized at 1 s interval, and is therefore used up to 0.02 Hz; at higher frequencies, our results could lose their robustness due to the possibility of an incorrect depth, and our modeling of lateral heterogeneity could become questionable (see *Okal and Talandier* [1989] for details). Nevertheless, it is clear that the

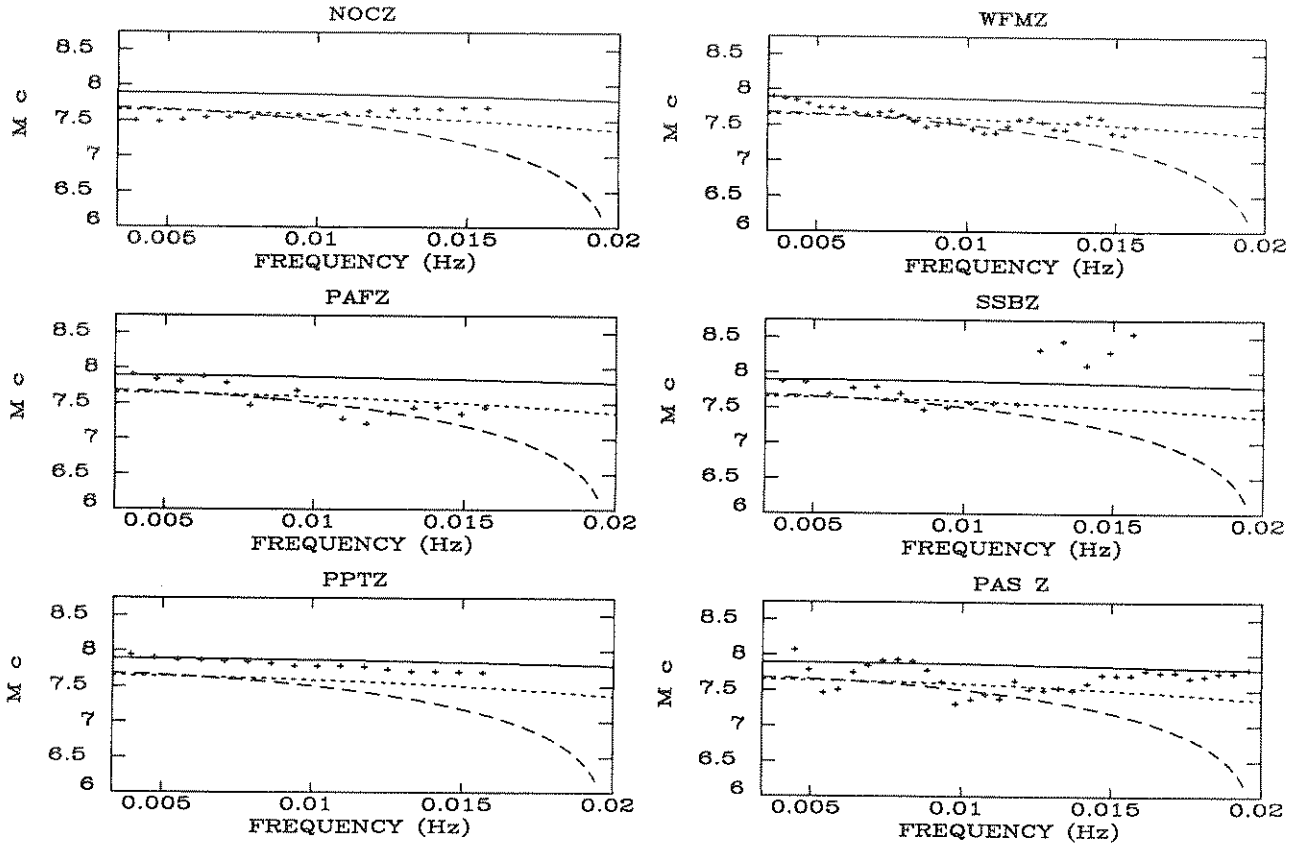

Fig. 16. Source spectra for the 1986 Kermadec earthquake, as derived from Rayleigh wave records. For each station, the plus signs are the spectral amplitudes at the individual frequencies (after correction for source excitation and propagation effects); the solid lines are the spectra expected from our derived values of M_0 and τ_s, the dashed and dotted lines, those expected from the solutions by *Romanowicz* [1988] and *Dziewonski et al.* [1987], respectively (see text for details).

source spectral amplitudes are inconsistent with a source duration of 50 s, this result being particularly evident at Nouméa (NOC), PPT and PAS. However, this dataset cannot help discriminate between the two shorter sources (30 and 19 s). As for the static seismic moment, all stations except NOC suggest a moment closer to the value we derive from the body-wave modeling than to the published CMT estimates.

We also attempted to model body waves with sources lasting 50 or 30 s. As shown in Figure 17, even a 30 s long source deteriorates significantly the fit of body wave shapes in the western stations (CHTO, MAJO). In interpreting the source time function obtained in Figure 15 as a single pulse of 19 s duration, we make the usual assumption that a negative value of the moment release rate results from computational artifacts and is not representative of rebound along the fault plane [*Lundgren*, 1988]. This assumption is indeed inherent, and negative moment release rates automatically zeroed, in a number of deconvolution codes described in the literature. As would be expected, we verified in an ndependent experiment that the fit between the early part of synthetics and observed data (especially at crucial stations such as COL and BOCO) would not be significantly degraded by limiting the source to the single, 19 s pulse shown in Figure 15.

We further studied the dimensions of the fault plane by plotting (in Figure 11*c*) the same-day aftershocks of the event. We eliminated from this figure those events described as "less accurate" (flagged by * in the NEIS catalog) or "questionable" (flagged by ?). The resulting cluster is oriented generally North-South, a trend in better agreement with the NNE-SSW striking focal plane than with its conjugate (E-W). The dimension of the aftershock zone thus defined is on the order of 80-100 km. Thus, the aftershock pattern suggests a unilateral rupture along the NNW trending focal plane. This plane is the better constrained one, and is practically common to all three mechanisms.

Relationship with Long-Term Aftershocks and Tectonic Interpretation

Figure 18 shows a map view and a cross-section of a 72-day sequence of aftershocks for which *Dziewonski et al.* [1987] published centroid moment tensor solutions ($m_b \geq 5.0$; $M_0 \geq 5 \times 10^{23}$ dyn-cm). Two features of this figure are remarkable: first, 30 out of 32 aftershocks occurred significantly shallower than the main shock ($h \leq 24$ km). Several depths given as 15 km may represent shallower values (D. Giardini, personal com-

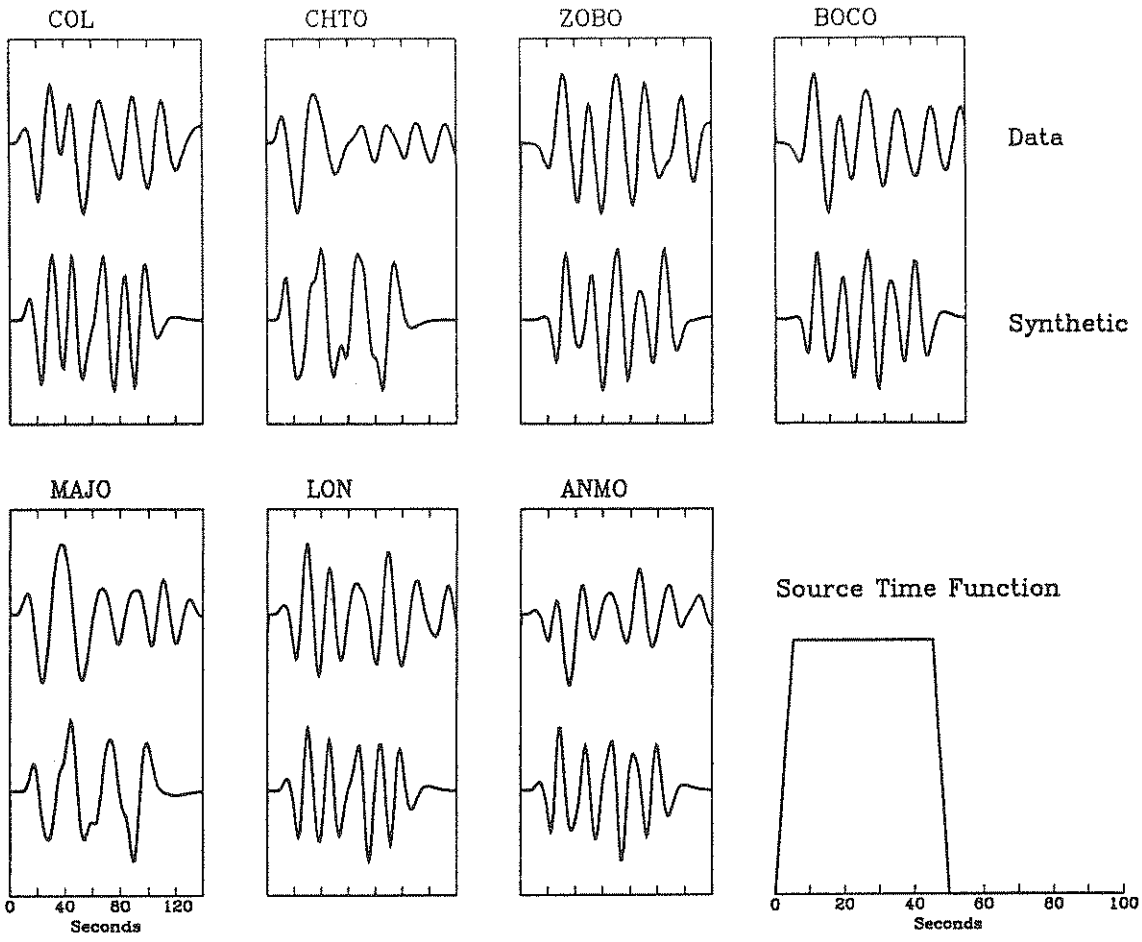
COL
CHTO
ZOBO
BOCO
Data
Synthetic
MAJO
LON
ANMO
Source Time Function
0 40 80 120
Seconds
0 20 40 60 80 100
Seconds
COL
CHTO
ANMO
BOCO
Data
Synthetic
MAJO
LON
ZOBO
Source Time Function
0 40 80 120
Seconds
0 20 40 60 80 100
Seconds

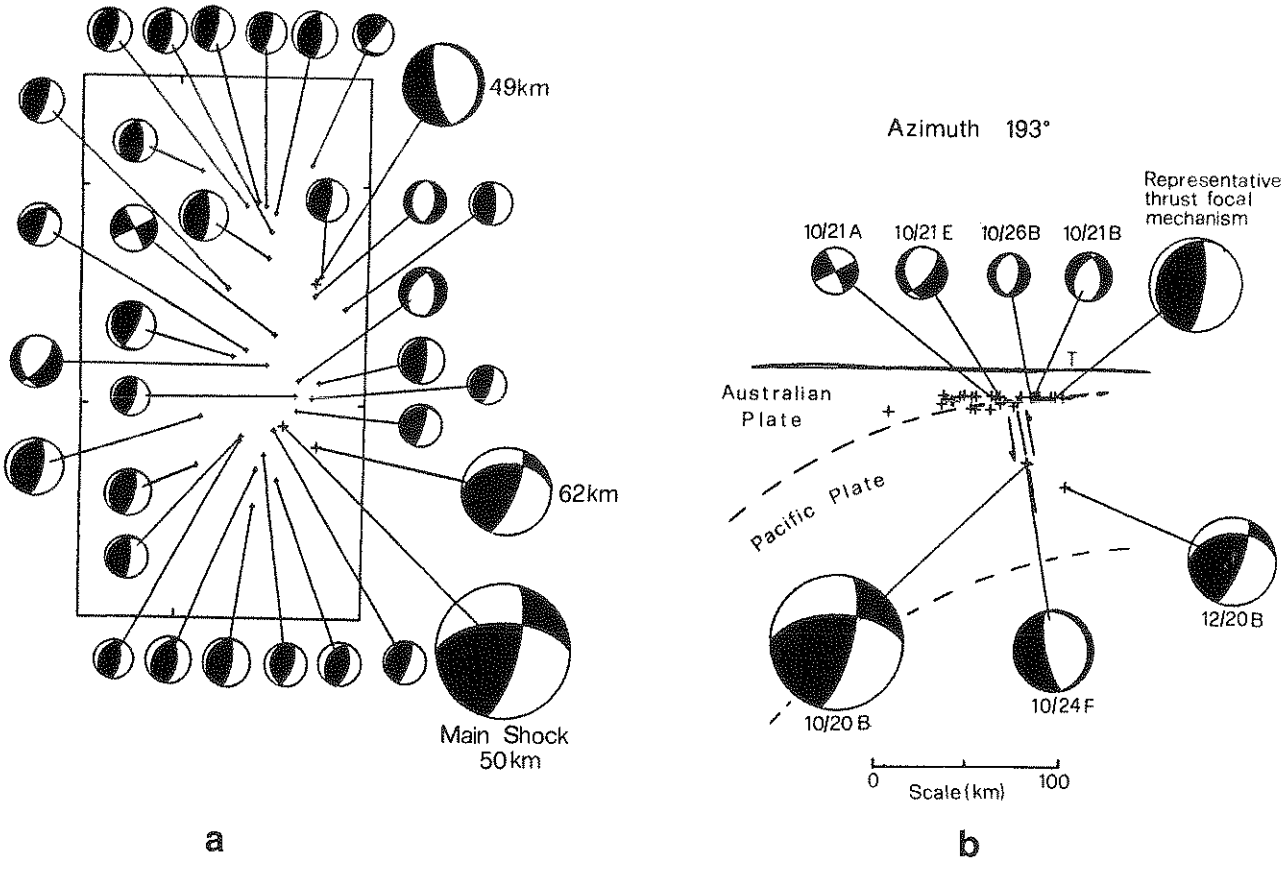

Fig. 18. (Left) Map of a 72-day sequence of aftershocks for which CMT solutions are available. (Right) Cross-section of the aftershock distribution along the azimuth N103°E. Focal mechanisms (represented as they would appear in map view), are given for the main shock, the two relatively deep aftershocks, and the four shallow events with non-thrust mechanism. As shown in the left panel, all other shallow events have a geometry comparable to the representative mechanism shown at upper right.

munication, 1988). In addition, only one relatively deep aftershock (122086B) shares the main shock's focal mechanism; 25 out of the 29 shallow events can be interpreted as reverse faulting on a shallow plane dipping arcwards approximately 20°; furthermore, there is some indication that the events themselves align at such an angle. This pattern clearly suggests that the main shock triggered a sequence of aftershocks, with both different location and mechanism.

According to the SYNBAPS dataset, the 1986 mainshock occurred 58 km arcwards of the trench, and its 40 km source depth puts it about 32 km deeper than the bottom of the Kermadec trench. It is difficult to assess the precise geometry of the downgoing Kermadec slab in the area. Although at greater depths, seismicity constrains the slab's dip to 65 ± 5° [*e.g., Uyeda and Kanamori,* 1979], it is much more difficult to map its shallower parts, in view of the large number of small earthquakes with imprecise source depths. In particular, the angle of subduction would be expected to grow smoothly with depth in the first few tens of kilometers, from 0° to its final value of 65°.

In this framework, we interpret the shallow, predominantly thrust events shown in Figure 18 as occurring at the interface between the Pacific and Australian plates. The main shock, therefore, must be viewed as an internal rupture of the Pacific plate. However, the interpretation of its mechanism is not simple. The compressional stress axis for the preferred mechanism dips only 17° at an azimuth of 134°, close to the direction of motion of the Pacific plate in the area, and thus generally compatible with the collision between the two plates at the subduction zone. The tensional axis (azimuth 240°; plunge 42°) deviates significantly from the direction of subduction, while the dip is far in excess of its local value for the slab, as discussed above. We propose to interpret the vertical component of the motion as the delamination of a sliver inside the Pacific plate under the release of compressional stress generated by the collision of the two plates (Figure 19). The strike-slip component is probably related to the obliquity of subduction in the area.

Fig. 17 (facing page). Attempt at modeling the 1986 Kermadec earthquake with a source time function 50 s (top) and 30 s (bottom) in duration. Otherwise, this figure is similar to Figure 15. Note significant deterioration in the quality of fit. This suggests a faster source for the 1986 earthquake.

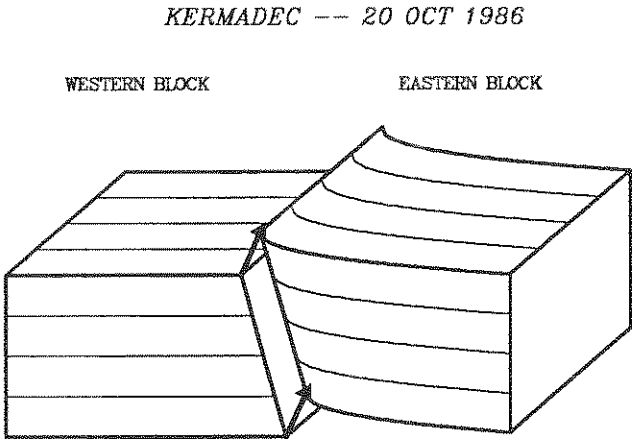

Fig. 19. Cartoon illustrating preferred interpretation of the focal mechanism of the 1986 Kermadec earthquake. Arrows show the direction of slip of the eastern block with respect to the western block, inside the Pacific slab.

The conjugate mechanism ($\phi_f = 268°$; $\delta = 47°$; $\lambda = 158°$) would be harder to interpret in terms of large-scale tectonic processes, since it would require faulting along an E-W striking plane, not supported by the aftershock distribution. Fault planes striking along the direction of subduction are known for slab-tearing events at the boundary between different geometries of subduction [*Lundgren et al.*, 1988; *Lundgren*, 1988]. However, these planes are usually vertical, with slip angles expressing the change in the slab's dip. In the present case, neither δ nor λ can be reconciled with this model.

In conclusion, we propose that the 1986 Kermadec earthquake represents a fast, clean, episode of overthrusting inside the Pacific plate at about 40 km depth, accompanied by a component of left-lateral strike-slip. This event later triggered aftershock activity at the nearby boundary between the slab and the Australian plate, in the form of regular thrust events, but on a much smaller scale, the total seismic moment released over 72 days being only 2.2×10^{26} dyn-cm, about 3% of that of the main shock. This kind of activity is reminiscent of the reactivation of decoupled subduction zones described by *Tajima and Célérier* [1989]; in this instance, however, it is post-seismic as opposed to coseismic in the cases they studied. It is not clear however that the earthquake took place in the fault area of a previous major shock. Figure 11 shows that no substantial seismicity had taken place in the epicentral area since 1963; the only very large event known in the area is the 1917 earthquake, with a reported magnitude $M = 8.6$ [*Gutenberg and Richter*, 1954], but its exact location is in doubt.

The short source duration suggested for the main shock by the body wave deconvolution ($\tau_s = 19$ s) and the extent of the aftershock zone suggest a velocity of rupture on the order of 4.5 km/s. While this number is high, it is comparable to the shear wave velocity at the hypocentral depth. When combined with the large moment suggested from this study (8.5×10^{27} dyn-cm), this yields a relatively high stress drop of 100 to 120 bars using the models of *Keilis-Borok* [1959] and *Geller* [1976]. The general character of this event emerging from these characteristics (high stress drop, reduced lateral dimensions and large rupture velocity) is reminiscent of *Silver and Jordan*'s [1983] conclusions regarding the 1977 Indonesian event (however, the latter occurred oceanwards of the trench). While we presently do not have an explanation for the process leading to its anomalous mechanism (which could, for example, involve the unusual buoyancy of a local heterogeneity in the Pacific plate, inhibiting its subduction), we suggest that its exceptional character is related to the high stress drop and small source dimensions documented in the present study.

5. CONCLUSIONS

We have presented two studies illustrating the important effect on teleseismic waveshapes of a system of dipping layers in the epicentral area. We suggest that, in the presence of significant dipping of the ocean floor, body-wave deconvolutions carried out under the inappropriate model of a flat-layered structure can lead to spurious complexity in the source time functions, and to incompatibilities between the source functions retrieved at individual stations.

In the case of the 1982 Tonga earthquake, we showed that by taking into account the dip of the ocean floor, it is possible to reconcile GDSN body wave shapes with a simple source time function consisting of a single pulse of moment release. As such, the event does not feature the previously suggested complex source function lasting for up to 100 s. In particular, the origin of the exceptional tsunami generated by this event is not a source duration effect, but rather the tsunami can be successfully modeled by a short-lived source propagating into the sedimentary wedge.

Similarly, in the case of the 1986 Kermadec earthquake, the introduction of a dipping near-source structure results in the retrieval of a very fast seismic source, consisting of a single pulse of 19 s duration. The unique combination of this figure, the large seismic moment and the anomalous focal mechanism of this earthquake suggests that the event represents internal scraping of a sliver inside the Pacific slab, under the ambient compressional stress field generated by the collision at the trench. The limited spatial and temporal extent of the source as well as the resulting high stress drop (100 to 120 bars) suggest that this anomaly in the subduction process may express the presence of an "unsubductible" local heterogeneity, of a possibly buoyant character. Its exact nature can only be speculated.

Acknowledgments. We thank Seth Stein and Domenico Giardini for discussion. We are grateful to John Woodhouse and Göran Ekström for updated versions of the Harvard CMT catalog, to Barbara Romanowicz for access to the GEOSCOPE dataset, and to Fumiko Tajima and Steven Ward for careful reviews. This research was supported by the National Science Foundation under grants EAR-84-05040, EAR-87-20549 (E.A.O.); EAR 86-18044 and EAR-87-21074 (D.A.W.); and the Petroleum Research Fund of the American Chemical Society, under Grant 17294-AC2 (E.A.O.).

REFERENCES

Abe, K., Tsunami and the mechanism of great earthquakes, *Phys. Earth Planet. Inter., 7,* 143-153, 1973.

Aki, K., Characterization of barriers on an earthquake fault, *J. Geophys. Res., 84,* 6140-6148, 1979.

Christensen, D.H., and T. Lay, Large earthquakes in the Tonga region associated with the subduction of the Louisville Ridge, *J. Geophys. Res., 93,* , 13367-13389, 1988.

Choy, G.L., and P.G. Richards, Pulse distortion and Hilbert transformation in multiply reflected and refracted body waves, *Bull. Seismol. Soc. Am., 65,* 55-70, 1975.

Dziewonski, A.M., A. Friedman, D. Giardini, and J.H. Woodhouse, Global seismicity of 1982: Centroid moment tensor solutions for 308 earthquakes, *Phys. Earth Planet. Inter., 33,* 76-90, 1983.

Dziewonski, A.M., G. Ekström, J.H. Woodhouse, and G. Zwart, Centroid moment-tensor solutions for October-December 1986, *Phys. Earth Planet. Inter., 48,* 5-17, 1987.

Fitch. T.J., Plate convergence, transcurrent faults, and internal deformation adjacent to Southeast Asia and the Western Pacific, *J. Geophys. Res., 77,* 4432-4460, 1972.

Fukao, Y., Tsunami earthquakes and subduction processes near deep-sea trenches, *J. Geophys. Res., 84,* 2303-2314, 1979.

Geller, R.J., Scaling relations for earthquake source parameters and magnitudes, *Bull. Seismol. Soc. Am., 66,* 1501-1523, 1976.

Gutenberg, B., and C.F. Richter, *Seismicity of the Earth and Associated Phenomena,* 310 pp., Princeton University Press, Princeton, N.J., 1954.

Houston, H., Source characteristics of large earthquakes at short periods, Ph.D. thesis, 148 pp., California Institute of Technology, Pasadena, 1987.

Kanamori, H., Mechanism of tsunami earthquakes, *Phys. Earth Planet. Inter., 6,* 346-359, 1972.

Kanamori, H., and J.J. Cipar, Focal process of the great Chilean earthquake, May 22, 1960, *Phys. Earth Planet. Inter., 9,* 128-136, 1974.

Kanamori, H., and J.W. Given, Use of long-period surface waves for rapid determination of earthquake-source parameters, *Phys. Earth Planet. Inter., 27,* 8-31, 1981.

Keilis-Borok, V.I., An estimation of the displacement in an earthquake source and of source dimensions, *Annal. Geofis., 12,* 205-214, 1959.

Kelleher, J., J. Savino, H. Rowlett, and W. McCann, Why and where great thrust earthquakes occur along island arcs, *J. Geophys. Res., 79,* 4889-4899, 1974.

Kikuchi, M., and Y. Fukao, Iterative deconvolution of complex body waves from great earthquakes – The Tokachi-Oki earthquake of 1968, *Phys. Earth Planet. Inter., 37,* 235-248, 1985.

Kikuchi, M., and H. Kanamori, Inversion of complex body waves, *Bull. Seismol. Soc. Am., 72,* 491-506, 1982.

Langston, C.A., The effect of planar dipping structure on source and receiver responses for constant ray parameter, *Bull. Seismol. Soc. Am., 67,* 1029-1050, 1977.

Lay, T., and H. Kanamori, An asperity model of great earthquake sequences, in: *Earthquake Prediction, Maurice Ewing Ser., 4,* edited by D.W. Simpson and P.G. Richards, pp. 579-592, AGU, Washington, D.C., 1981.

Lundgren, P.R., Deformation at subducting slabs at intermediate depths (abstract), *Eos, Trans. AGU, 69,* 1316, 1988.

Lundgren, P.R., and E.A. Okal, Slab decoupling in the Tonga arc: The June 22, 1977 earthquake, *J. Geophys. Res., 93,* 13355-13366, 1988.

Lundgren, P.R., E.A. Okal, and S. Stein, Body wave deconvolution for variable source parameters; application to the December 6, 1978 Kuriles earthquake, *Geophys. J., 94,* 171-180, 1988.

Okal, E.A., Seismic parameters controlling far-field tsunami amplitudes: A review, *Natural Hazards, 1,* 67-96, 1988.

Okal, E.A., and J. Talandier, M_m: Theory of a variable-period mantle magnitude, *Geophys. Res. Lett., 14,* 836-839, 1987.

Okal, E.A., and J. Talandier, M_m: A variable-period mantle magnitude, *J. Geophys. Res., 94,* 4169-4193, 1989.

Romanowicz, B.A., Centroid moment tensor solutions of recent events from GEOSCOPE data, paper presented at Annual Meeting, Europ. Geophys. Soc., Bologna, Mar. 14-18, 1988.

Ruff, L.J., and H. Kanamori, The rupture process and asperity distribution of three great earthquakes from long-period diffracted *P* waves, *Phys. Earth Planet. Inter., 31,* 202-230, 1983.

Silver, P.G., and T.H. Jordan, Total-moment spectra of fourteen large earthquakes, *J. Geophys. Res., 88,* 3273-3293, 1983.

Stein, S., and D.A. Wiens, Depth determination for shallow teleseismic earthquakes: methods and results, *Rev. Geophys., 24,* 806-832, 1986.

Tajima, F., and B. Célérier, Possible focal mechanism change during reactivation of a previously ruptured subduction zone and stress tensor implications, *Geophys. J. Intl., 98,* 301-316, 1989.

Talandier, J., and E.A. Okal, Human perception of *T* waves: the June 22, 1977 Tonga earthquake felt on Tahiti, *Bull. Seismol. Soc. Am., 69,* 1475-1486, 1979.

Talandier, J., and E.A. Okal, An algorithm for automated tsunami warning in French Polynesia, based on mantle magnitudes, *Bull. Seismol. Soc. Am., 79,* 1177-1193, 1989.

Talandier, J., D. Reymond, and E.A. Okal, M_m: Use of a variable-period mantle magnitude for the rapid one-station estimation of teleseismic moments, *Geophys. Res. Lett., 14,* 840-843, 1987.

Uyeda, S., and H. Kanamori, Back-arc opening and the mode of subduction, *J. Geophys. Res., 84,* 1049-1061, 1979.

Ward, S.N., Ringing *P* waves and submarine faulting, *J. Geophys. Res., 84,* 3057-3062, 1979.

Wiens, D.A., Effects of near source bathymetry on teleseismic *P* waveforms, *Geophys. Res. Lett., 14,* 761-764, 1987.

Wiens, D.A., Bathymetric effects on body waveforms from shallow subduction zone earthquakes and application to seismic processes in the Kurile trench, *J. Geophys. Res., 94,* 2955-2972, 1989.

P.R. Lundgren, Mail Stop 183-501, Jet Propulsion Laboratory, 4800 Oak Grove Drive, Pasadena, California 91109.

E.A. Okal, Department of Geological Sciences, Northwestern University, Evanston, Illinois 60208.

D.A. Wiens, Department of Earth and Planetary Sciences, Washington University, Saint Louis, Missouri 63130.

(Received March 3, 1989;
revised June 9, 1989;
accepted June 12, 1989.)